EAF Heat Recovery from Incident Radiation on Water-Cooled Panels Using a Thermophotovoltaic System: A Conceptual Study

Yadollah Saboohi, Amorhossein Fathi, Igor Škrjanc, and Vito Logar*

In this paper, a conceptual study and quantification of using a thermophotovoltaic system (TPV) to convert incident radiation on furnace panels to electrical energy is presented. In typical electric arc furnaces, a considerable amount of energy is wasted during the melting process, that is, steel enthalpy, off-gas extraction, vessel cooling, slag enthalpy, and others. Although a remarkable share of the energy is wasted in circulating water, the contained exergy is simply too low to be considered for heat recovery (under 0.5% of input exergy) in comparison to energy content of the extracted gasses and slag. In the performed study, a TPV power output is calculated as a function of arc length, slag and bath height, zone temperatures, and emissivities. Two major changes to the existent EAF model were performed in order to estimate the TPV efficiency, that is, 1) the radiative heat transfer module has been re-developed to allow calculation of the incident radiation on the TPV, 2) the model has been extended with a TPV module, which is used to estimate the electricity produced by the TPV. The effects of TPV capacity, its distance from the slag layer and input regime on generated electrical energy are studied. The results have shown that a typical EAF, equipped with TPV system, can reduce average energy consumption by 4.8 kWh ton^{-1}, which corresponds to approximately 0.8% overall efficiency improvement. Moreover, the capacity factor of the installed TPV is predicted at 54% over a period of one year.

1. Introduction

Steel industry ranks as second in overall energy consumption (about 21%) and CO_2 emissions (about 30%) in the industrial sector.[1] Studies have shown that steel demand is likely to increase for approximately 150% by 2050 when compared to 2013.[2] A typical EAF consumes approximately 450 to 550 kWh of electric energy per ton of steel produced. For this reason, different strategies and technologies on partial energy recovery have been introduced or are still being investigated.[3–5] Management and optimal operation, improvement of raw materials quality, improvement of technology, and heat recovery systems were the key factors to reduce the energy intensity for almost 60% in past five decades.[2] Implementation of a heat recovery system to the EAF represents a huge advantage, since it converts energy, which would otherwise be lost, into useful energy without (or with low) CO_2 emissions. The major part of the energy consumed in a batch is wasted in slag, off-gas, and water-cooled panels. So far, many studies have been developed to recover a part of those losses in off-gas[3] and slag.[4] Although the energy loss in water-cooled panels is estimated to be up to 306 kWh ton^{-1} (equivalent to 40% of the input energy),[5] energy recovery from water-cooled panels is not profitable, due to exiguous share in exergy flow, which is estimated at approximately 0.3%.[6]

For the above reason, the idea of the study is to investigate, whether the energy, transferred to the water-cooled panels, can partially be recovered using a thermophotovoltaic system (TPV). A TPV is a high power density conversion technology, which generates electrical energy from radiation emitted by a heated body.[7] In a typical EAF layout, a part of the upper-wall zone, which is not covered by the slag or dust, can be qualified for energy recovery via a TPV.

Since early 1960, numerous studies have been performed on structure and material properties in order to improve the TPV performance and power density.[8–10] The research has led to a TPV development, for which the TPV is nowaday considered as a reasonable heat recovery technology in high temperature processes. Three places in a high-temperature process can be considered as reasonable area to install the TPV, that is, product, by-product (flue gas), heated walls, and body.[11]

Many studies have been carried out to evaluate the TPV structure and its role in energy recovery. Bauer et al.[12] provided a general review on TPV recovery potential in the UK industry. Its energy recovery potential and the consequent reduction of CO_2 emissions are apprised in the high-temperature industry in

Prof. Y. Saboohi, Dr. A. Fathi
Sharif Energy Research Institute (SERI)
Sharif University of Technology
Azadi Ave, Tehran, 1459777611, Iran
E-mail: fathi@seri.sharif.edu

Prof. I. Skrjanc, Assis. Prof. V. Logar
Faculty of Electrical Engineering
Laboratory of Modelling
Simulation and Control (LMSV)
University of Ljubljana
Tržaška 25, SI-1000, Ljubljana, Slovenia

DOI: 10.1002/srin.201700446

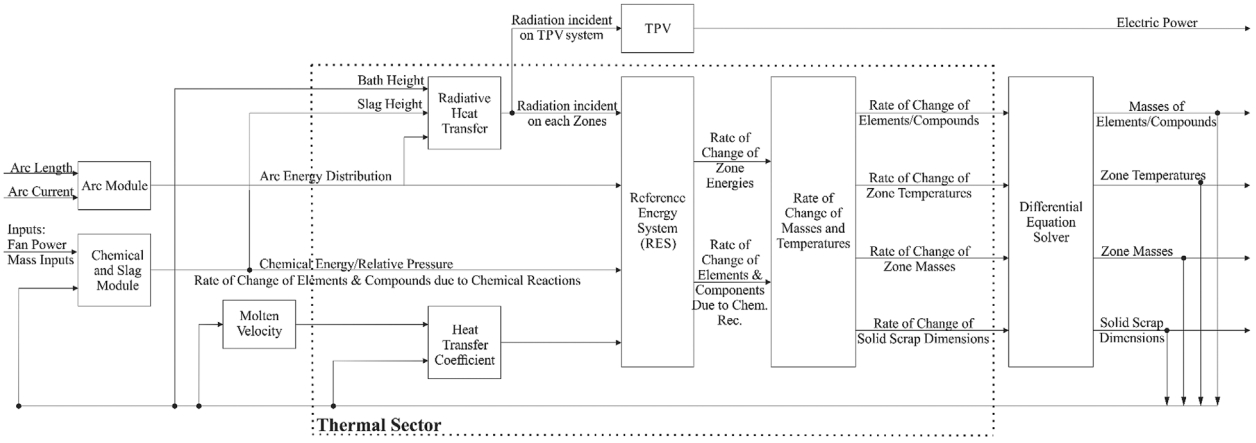

Figure 1. Block diagram of the EAF model with additional TPV module.

the UK. A similar study has been performed by Utlu and Parali,[13] who evaluated the TPV potential of energy recovery from different high-temperature processes in Turkey. An estimation of the high-temperature energy losses in different industry categories has been performed, and approximate energy savings are estimated according to three possible scenarios of TPV efficiency. The heat recovery potential is estimated in a range from 6.22 to 18.74 TWh yr^{-1}, depending on the TPV efficiencies. Furthermore, another study performed by Bauer et al.[14] assessed the TPV heat recovery potential for a glass industry in the UK. Frass et al.[15] investigate power generation potential using a TPV system in a steel mill producing 10 MT steel per year. Power recovery potential of 20 MW in average is reported. Regarding the performed studies, it can be concluded that TPV systems have a huge potential in energy recovery for the high-temperature processes.

Studying the effect of a TPV system on the recovered energy requires a simulation model capable of estimating the radiative heat transfer to TPV. Power density generated by the TPV is a function of different factors related to the properties of the surfaces forming an EAF enclosure and a TPV system: surface parameters; temperatures, emissivities and areas, TPV efficiency etc. In the EAF, most of these factors vary during the heat, in contrast to the steel mill. Therefore, a radiative module should be integrated into an EAF simulation model, which estimates dynamic behavior of the EAF and its influence on electrical energy generation. Fathi et al.[16] presented an EAF simulation model, where furnace layout has been described by 11 main zones. Six of them form an enclosure and are contributing to the exchange of energy through radiation mechanism, that is, arc – *arc*, electrodes – *electrode*, roof – *roof*, liquid slag – *lSl*, the lower-wall zone or refractory brick – *wall* and upper-wall zone or water cooled panels – *water*. The model utilizes an arc module based on channel arc model to enhance estimation of the arc energy distribution and arc shape. Surface geometries inside the EAF are simplified, since there are no validated studies to estimate the surface geometry changes.

Even though the radiative heat transfer module is already developed, it should be modified to allow computation of the energy received by the TPV. Furthermore, a TPV module should be added to the EAF model to calculate the generated power by the TPV over time. The conceptual model of the EAF equipped with the TPV is revised according to **Figure 1**.

2. Modeling

A TPV is a system, which utilizes conversion technology to generate electrical energy from incident radiation. A typical TPV assembly consists of three parts, that is, the needed source emitting radiative heat, optical system (filter and reflecting frame) to minimize radiation losses, and a photovoltaic (PV) system to convert radiation into electric power.[17] Generally, a TPV output can be computed in four steps: first, radiation power of the source needs to be determined according to the heating technology efficiency; second, the share of radiation power transferred to the TPV has to be calculated using the view factors from the source to the TPV, according to optical efficiency of the TPV; third, a share of received radiation power that can be converted into electrical energy is obtained based on spectral efficiency; and fourth, electrical power produced by the TPV is determined according to the efficiency of the PV cells.

When considering an EAF, the sources of radiation with significant heat contribution are the arcs, slag, electrodes, and lower side wall. In this paper, radiative heat transfer module is used to determine the incident radiation on the TPV. Further, a TPV module is applied to estimate the produced electrical power according to the incident radiation on the TPV.

In order to take full advantage of the integrated TPV, the system should be placed in a manner that maximizes the view factors from the main heat sources, thus receiving maximum radiation. However, negative impacts of the slag and dust contact should also be considered. **Figure 2** shows the proposed placement of a TPV into an EAF assembly.

As can be seen in Figure 2, the TPV should not cover the complete upper wall zone. A gap in the wall zone is intended to prevent damage to the TPV system arising from the slag's corrosive characteristics. Moreover, installing a TPV on the furnace roof is not reasonable, since the generated power of the TPV is too low. As Figure 2 shows, placement of the TPV should be between the denoted areas $water_1$ and $water_2$. Such division

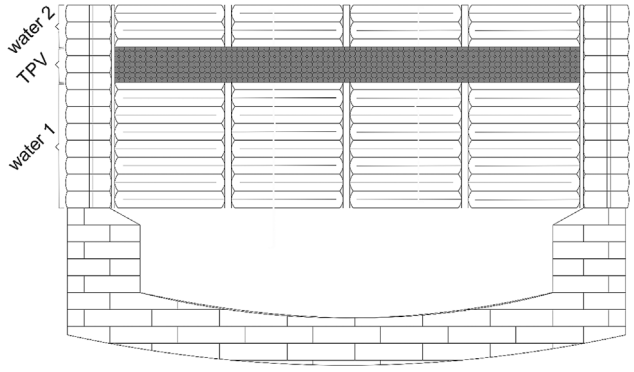

Figure 2. Schematic representation of an EAF equipped with a TPV system.

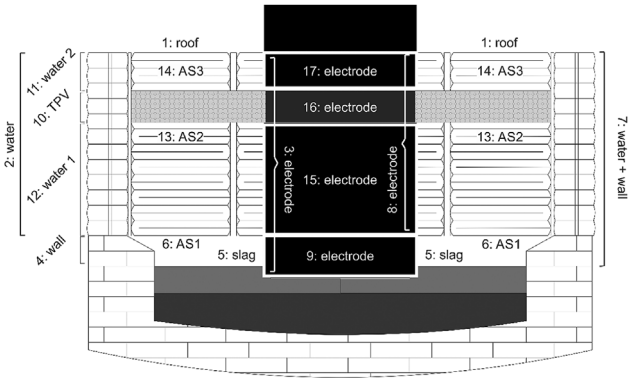

Figure 3. EAF zones used to calculate the view-factors and radiative heat.

gives the opportunity to determine the optimal TPV area for a given EAF using a suitable optimization methodology.

2.1. Radiative Heat Transfer

According to the simplified geometries considered for a typical EAF, up to eight surfaces can be formed in the EAF enclosure. During the melting, variations in slag height, bath height, and arc length can cause the number of surfaces to change. Also possible, slag can cover *arc*, $water_1$ and *wall* zones.

The radiative heat transfer module described in Fathi et al.[16] counts all surfaces (excluding the *arc*) as gray bodies and utilizes Stefan-Boltzman law to compute the radiosity of surfaces, as described by Equation (1). In contrast to some studies, such as Opitz et al.,[18] emission and absorption of off-gas is neglected.

$$(J_i - \sigma_B T_i^4)\frac{NA_i\varepsilon_i}{1-\varepsilon_i} + \sum_{j,j\neq i}(J_i - J_i)NA_i VF_{ij} = 0. \quad (1)$$

Table 1. View factor calculation procedure.

	Surface	Main VF − Direct	Other VF	Main VF
1	1-(16–17)-11-10-13	VF_{1-10}, VF_{1-11}	VF_{10-12}, VF_{10-16}	
		$VF_{10-1}, VF_{10-10}, VF_{10-11}$	VF_{10-11}	
		VF_{11-1}, VF_{11-10}	$VF_{11-(16-17)}$	
			VF_{11-11}	
			VF_{11-17}	
			VF_{11-1}, VF_{1-11}	
			VF_{11-10}	
2	14-(15–16)-10-12-6	VF_{10-12}, VF_{12-10}	$VF_{10-(15-16)}$	
			$VF_{12-(15-16)}$	
			VF_{12-15}	
3	13-(9–15)-12-4-5	VF_{4-4}, VF_{4-12}	$VF_{4-(9-15)}$	
		VF_{5-12}		
		$VF_{12-4}, VF_{12-5}, VF_{12-12}$		
4	1-2-3-4-5	$VF_{1-1}, VF_{1-3}, VF_{1-4}, VF_{1-5}$		VF_{1-12}
		$VF_{3-1}, VF_{3-3}, VF_{3-4}, VF_{3-5}$		VF_{12-1}
		$VF_{4-1}, VF_{4-3}, VF_{4-4}, VF_{4-5}$		
		$VF_{5-1}, VF_{5-3}, VF_{5-4}, VF_{5-5}$		
5	14-(9-15-16)5(4–12)-10	VF_{5-10}	$VF_{10-(4-12)}$	VF_{5-11}, VF_{11-5}
		VF_{10-5}		VF_{10-4}, VF_{4-10}
		VF_{11-11}		VF_{11-4}, VF_{4-11}
6	1-3-5(4-10-12)-11	VF_{3-11}, VF_{11-3}		VF_{11-12}, VF_{12-11}
				VF_{10-3}, VF_{3-10}
				VF_{3-12}, VF_{12-3}

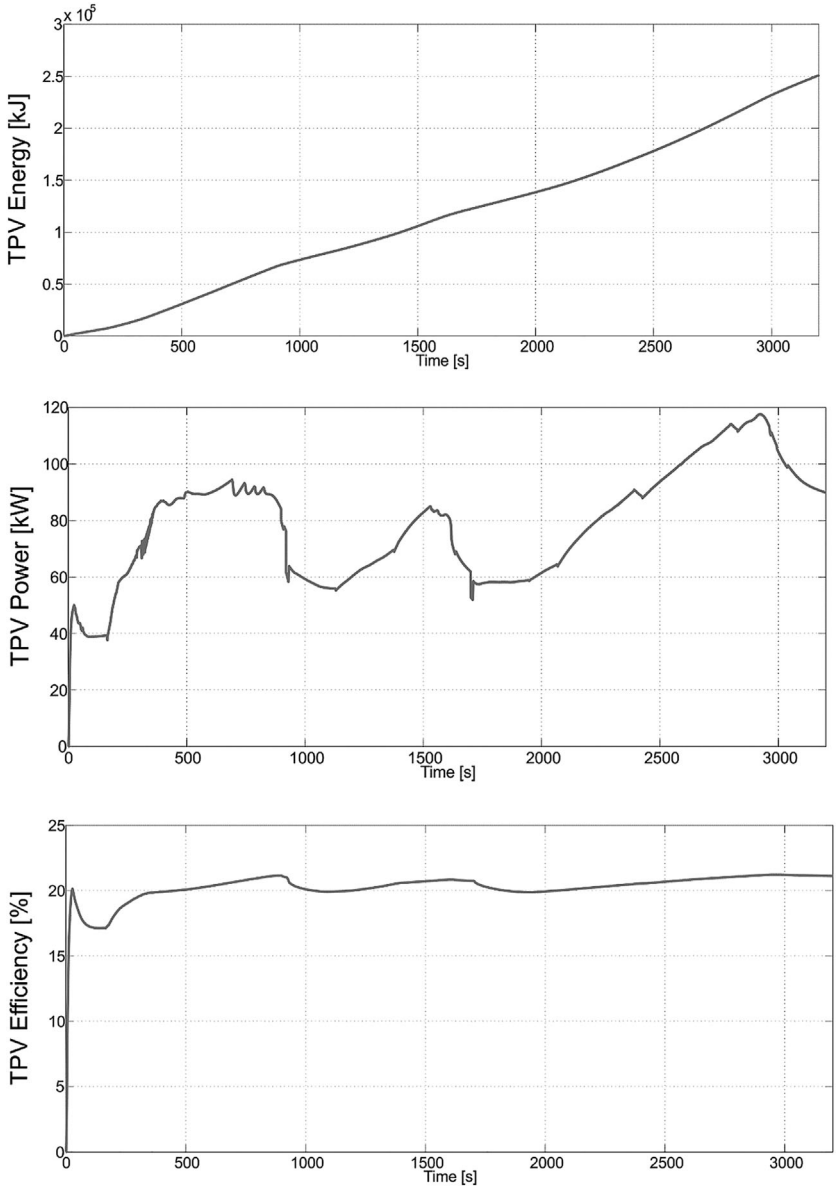

Figure 4. TPV energy, power, and efficiency during the heat.

The arc, similar as in studies,[19,20] is assumed as a black body when receiving radiative heat and acts as a transparent body when emitting radiative heat. In our previous works, the EAF layout was divided into six surfaces regarding the radiative heat calculations; however, in this study eighteen zones are defined in order to obtain more accurate results. Arc radiation on different zones is calculated separately, based on the results presented in ref.[21] When determining overall radiative impact to a zone, first, radiative heat transfers between the surfaces (except the *arc*) are determined using Equation (2), followed by the addition of the arcs' radiative heat dissipated to other surfaces.

$$Q_{Rad_{i-j}} = \left(J_i - J_j\right) NA_i VF_{i-j}, \tag{2}$$

where VF_{i-j} is the view factor between surfaces i and j, ε_i is emissivity of surface i, σ_B is Stefan-Boltzman constant, J_i is radiosity of zone i, NA_i is the area of a surface i that reaches out of the slag and bath zone and is located inside the EAF and $Q_{Rad_{i-j}}$ represent energy transferred from surface i to surface j through the radiation mechanism.

This simplification is used in order to reduce the computational load, especially when obtaining view factors and surface radiosity. The view factors are extracted from refs.[19,22] using the reciprocity relation, superposition rule, symmetry rule, and summation rule.

In the proposed methodology, we consider an EAF layout divided into eighteen surfaces for the radiative heat exchange calculations, as shown in **Figure 3**.

Positioning a TPV system in the middle of the upper side wall adds two other zones in the calculations. The challenging issue is to properly determine the view factors. Geometries assumed for surfaces are similar to the previous work.[16] Walls, two parts of the cooling panels, TPV area, and electrodes are assumed to have a cylindrical shape, while the roof and the liquid slag surfaces are considered to have a ring shape.

In Figure 3, AS1 is assumed as a virtual surface, which is parallel with the slag surface and passes the interface between wall and water. AS2 is also assumed as a virtual surface similar to AS1, which passes the interface between the *TPV* and $water_1$ zones. AS3 is also assumed as a virtual surface, which cuts the interface between $water_2$ and *TPV* zones. The three virtual surfaces divide the electrodes into four parts, as shown in Figure 3. In order to calculate the radiative heat transfers, view factors between surfaces numbered with 1, 11, 3, 4, 5, 10, and 12 are required. These view factors can be obtained considering the internal surfaces of the EAF in six possible configurations, which are shown in **Table 1** together with the view factors calculated in each step and in each configuration.

In Table 1, "Main VF − Direct" represents the view factors between two main surfaces numbered with 1, 11, 3, 4, 5, 10, and 12. "Other VF" represents the supplemental view factors between the surfaces that need to be known in order to calculate some of the main view factors that cannot be obtained directly with the six defined configurations. "Main VF" represents the main view factors, which cannot be obtained directly with one of the six configurations, but are obtained using the reciprocity relation, superposition rule, symmetry rule, summation rule, "Main VF − Direct", and "Other VF". The number denotes the corresponding surface. The numbers that are located in the parenthesis show the VF, which is obtained with the

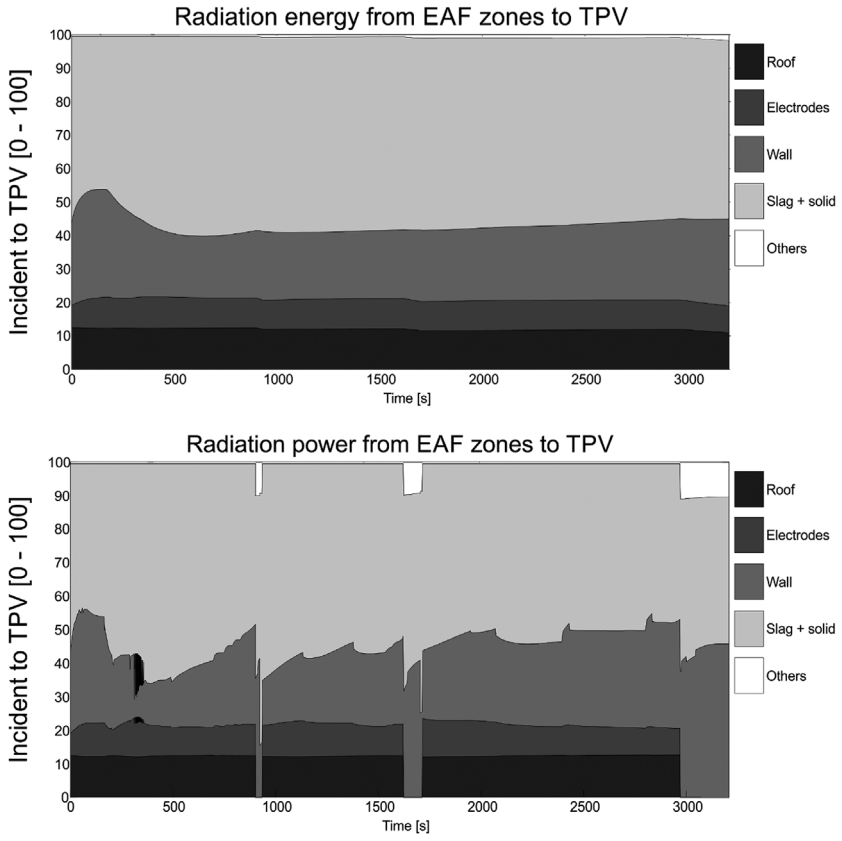

Figure 5. Shares of radiative energy/power from different zones to overall energy/power of the TPV.

combination of those surfaces. After calculating the view factors, eight equations are solved to find eight surface radiosities. VF equations used in this study are accessible in appendix 1.

At this point, the presented model does not consider the influence of off-gas and its dust load emission and absorption to radiative heat transfer. The reason for this is twofold. First, although the physical background of gas radiation is well known, it is practically impossible to validate the mathematical model describing this phenomena due to inexistent measurements of the influential variables. Consequently, indirect validation of the model could be possible by using measurements of off-gas composition, temperature, and water-cooled panels temperatures, the later also being used to validate the existent radiation model.[19,23] However, estimation of the gas-radiation share to overall radiative heat would be relatively unreliable. Second, regarding the conditions in the EAF during typical operation, the impact of the gas-radiation to the TPV is in our opinion not as important as the impact of other radiation emitters (electrodes, slag, scrap). The reason for this is that off-gas temperature is usually very close to those of slag and scrap and its absorptivity and emissivity should be very close to each other. As such, the off-gas radiation has only a minor influence to the TPV.

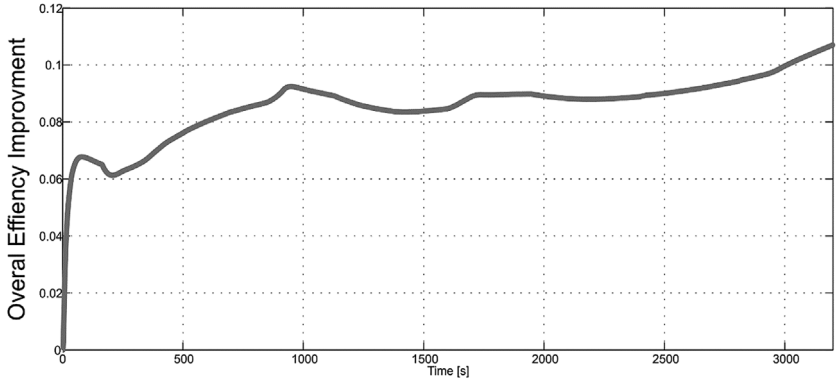

Figure 6. The effect of TPV on overall heat efficiency.

2.2. TPV Module

The TPV module is used to estimate the performance of the two TPV units, that is, the optical system and the photovoltaic system. Photons hitting the PV cells can generate current, if their energy is higher than the semiconductor band gap. Otherwise, overall efficiency of the system is reduced, since a TPV system requires a spectral control system, which passes the radiation with wavelengths lower than those of the photovoltaic band gap wavelength and reflects the other. Some indexes, such as Chubb index,[24] are used to evaluate the spectral tuning level.[25] A spectral system can consist of four sub-units: emitter, filter, anti-reflection layer, and reflector.[17] The overall efficiency of a spectral unit is defined by dividing the input power received by the TPV ($\overline{Q_C}$), with total radiation transferred to the TPV ($\overline{Q_E}$) as described by Equation (3).[25]

$$\eta_{spectral} = \frac{\bar{Q_C}}{\bar{Q_E}} = \frac{A_C \int_0^{\lambda_g} q_{iC}(\lambda, T) d\lambda}{A_F \int_0^{\infty} q_{oE}(\lambda, T) d\lambda}, \tag{3}$$

where A_C and A_E represent the area of the collector and the emitter, respectively, λ_g is the photovoltaic band gap wavelength, q_{iC} is radiation transferrring to the PV, and q_{oE} is radiation leaving the emitter.

The PV unit is intended to generate electric power from the input radiation. Its efficiency is obtained using Equation (4).[13,25]

$$\eta_{PV} = \frac{V_{OC} J_{SC} FF}{A_C \int_0^{\lambda_g} q_{iC}(\lambda, T) d\lambda,} \tag{4}$$

where V_{OC} is the open voltage, $J_{SC}$is the short circut current and FF, represents the fill factor.

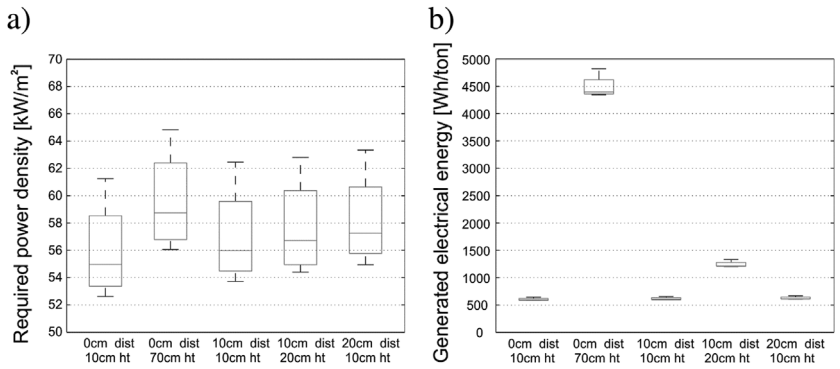

Figure 7. a) Required power density and b) electrical energy generated of the TPV according to its height and position.

When selecting a proper PV system, its band gap characteristics play the key factor to determine its application. A PV cell can be divided into three groups, based on the band gap characteristics, that is, high band gap, middle band gap, and low band gap. According to this category, proper application of the PV can be determined. High band gap PV (around 1.1 eV) is based on silicon and applicable for ultra high emitter temperature (over 1800 K). Middle band gap PV (around 0.7 eV) require the emitter temperatures in the range from 1273 to 1873 K, in order to have a satisfactory output. The most popular strucures in this group are GaSb cell (developed technology), Ge cell with W spectra (nearly developed technology), InGaSb on InP (developing technology), and InGaAsSb on GaSb (developing technology). Low band gap PV (less than 0.5 eV) is used when low temperatures of the emitter are present. The structure is mostly based on quaternery simicondutors such as InAsPSb on GaSb.[17,25]

In conceptual and feasibility studies, it is convenient to use constant values to desribe efficiency.[12,13] The manufacturers of PV systems usually present the unit's efficiency according to its application. For example, Jx Crystal Inc.[26] reported that efficiency of a TPV system, based on a single GaSb cell with 1.5 $\frac{W}{cm^2}$ power and the emitter temperature of 1548 K, is 21.5%. Spectral efficiency and cell efficiency are reported to be 29 and 74%, respectively.

In order to achieve proper operation and use the potential of the TPV, special attention must be devoted to the installation of the system in terms of its size, positioning, and proper cooling. The three main concerns when using such a system in an EAF environment are the following. First, can the system withstand high temperature loads from gasses, dust, and burners? Second, can splashing slag and its freezing to TPV be avoided? And third, can mechanical damage from scrap charging be prevented?

Regarding the temperature resistance of the TPV (gas, dust, and burner flames), the emitter is at this point not problematic, as it can withstand the temperature levels in an EAF. On the other hand, internal components of the TPV are not designed for high temperatures and should, therefore, be properly cooled. Since the research presented in this paper is still in the conceptual stage, an exact design of the cooling system cannot be shown, as it is a subject to extensive testing in real environments. However, a combination of air- and water-cooling as suggested by Fraas[15] could be used to provide sufficiently low temperatures for the TPV components and avoid damage caused by excessive heat.

In order to prevent slag splashing and mechanical damage to the TPV, its size and positioning are crucial. For this reason, this study suggests to design a relatively narrow panel, which should be positioned around the furnace circumference just below the furnace roof. In this manner, the distance between the slag and the TPV should be large enough to prevent or at least minimize slag splashing and freezing to the TPV. Nonetheless, occasional splashes of slag could occur, therefore the TPV emitter should be designed in a manner that withstands slag splashes and allows simple slag removal and/or its replacement. Similarly, the thickness of the emitter should be large enough to withstand EAF charging and occasional steel impacts.

3. Results

In order to suggest proper selection of the TPV system, calculate its efficiency, and heat recovery potential, the calculations have been performed based on measured data of different heats of a modern EAF. The data and the properties of the EAF have already been reported in refs.[16,23] TPV efficiency function was extracted from **Figure 6** in ref.[25] using a suitable software (Plot Digitizer[27]). The hotter side of the TPV is assumed to have a temperature, which is the average of gas and water cooled panel temperatures.

In the first evaluation, a TPV is positioned at a distance of 10 cm from the furnace roof and is assumed to have a height of 10 cm. **Figure 4** shows energy, power, and efficiency of the TPV during the heat.

As can be seen in Figure 4, a TPV can save up to 0.66 $\frac{kWh}{Ton_{lSc}}$, with a power density higher than 56.7 $\frac{kW}{m^2}$ and the expected average efficiency up to 20.2%. Capacity factors for a single heat and a

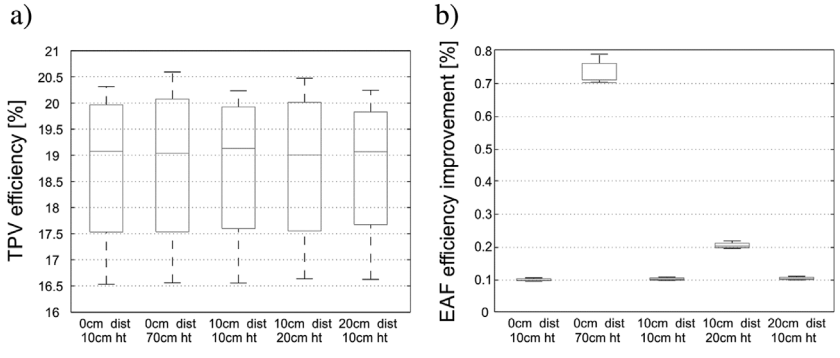

Figure 8. a) Efficiency of the TPV and b) overall EAF efficiency improvement according to the TPV height and position.

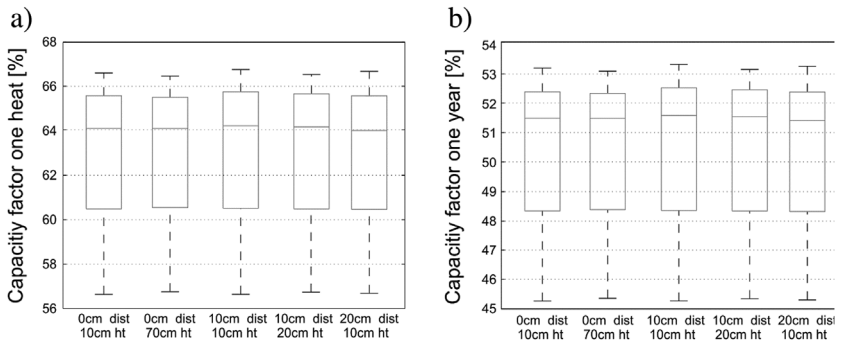

Figure 9. a) Single heat and b) annual capacity factors of a TPV according to its height and position.

one year period are estimated at approximately 66.7 and 53.4%, respectively. Such capacity factors are comparable with the capacity factors reported for fossil − fuel (except coal) renewable power plants.[28]

The share of different inputs to the energy/power produced by a TPV is shown in **Figure 5**.

As seen in Figure 5, the main energy sources to the TPV are the slag, solid scrap and the wall zones, with a share of 53.5 and 25.9%, respectively. In order to simplify the calculations, slag and solid scrap radiations are considered as one. The reason for this simplification is that only one of them is exposed at the same time in terms of radiation to TPV during a normal EAF operation.

Also visible in Figure 5, radiative heat from the arcs to TPV has been neglected. The reason for this is that view factors between the arcs and the TPV are zero for most of the time, meaning that there is no significant exposure of the system to arc radiation. The VFs are greater than zero only for a short periods of time in the beginning of each charge until the arcs bore into the scrap. Otherwise, they're either covered by solid scrap or foamy slag. As such, the direct effect of the arcs to the TPV can be omitted in the calculations to simplify the model.

The next thing that needs to be explained is the view factor between the wall zone and the TPV at the beginning of the charge. As can be seen in Figure 5, the VF between the walls and the TPV is not zero in the beginning of the heat as one would expect due to charged scrap. Regarding the dimensions of the studied EAF and the characteristics of the charged scrap (weight and bulk density), the scrap never reaches over the furnace walls, which explains why the wall zone is already visible to the TPV from the beginning of the heat and also at each basket charging.

Figure 6 represents the effect of a TPV on the efficiency of a single heat.

The required power density of a TPV, its energy conversion efficiency, electrical energy generated during a heat, EAF efficiency improvement and capacity factors (during a heat and as well as a year) are all dependent on TPV installation locations, installed TPV capacity, and EAF operating regime. **Figure 7**–11 are used to visualize the above indices as a function of nine different TPV locations and capacities and four typical heats of a 105 ton EAF.[16,23] TPV distance from the roof and its height are marked as "dist" and "ht", respectively.

Figure 7a shows that whenever the distance between the TPV and the slag zone is decreased (due to either increased TPV height or distance to the roof), the required TPV power density is increased. Maximum required power density for implementation to the EAF is predicted to be 70 $\frac{kW}{m^2}$. Although the power density is high, according to the literature,[29] such TPVs are available. Figure 7b shows the electrical energy generated by the TPV. As expected, increasing the TPV's height (equivalent to increased capacity of the installed TPV) and decreasing the distance between the TPV and slag (equivalent to increased input energy density) leads to increased generation of the electrical energy, which is a consequence of slag being the main emitter of the radiative heat incident on the TPV.

Average TPV energy conversion efficiency is presented in **Figure 8**a and overall increase in EAF efficiency is presented in Figure 8b.

The predicted TPV efficiency is in the range from 16.5 to 20.7% (in average of 18.8%). Similar efficiencies can be found in other energy conversion technologies, such as waste-to-energy (22–28%), dish stirling (18–23%), and small micro turbines (17–22%).[30]

Figure 9 shows the capacity factor of the TPV installed on the water cooled panels.

As shown in Figure 9a, the capacity factor of a TPV for the studied EAF is in the range of 56–66%. The expected annual capacity factor is shown in Figure 9b (assuming that TPV does not cause failures that lead to lower production). As shown in Figure 9b, the annual capacity factor is in the range of 45–54% (in average of 50.5%). Such factors are comparable to other energy conversion technologies, such as coal steam plants and combined cycle plants.[31]

Due to recovered radiative heat, the TPV also reduces CO_2 emissions, since the generated electrical energy can be reused and substitutes the electrical energy taken from the grid.

4. Conclusion

In this paper, a conceptual simulation study on TPV usage in modern EAFs is performed. The idea of using a TPV is to recover a part of the radiative heat, which would otherwise be lost in the water cooled panels and in this manner reduce the energy demand of the EAF. Heat recovery from the water cooled panels is not an interesting solution due to negligible exergy. On the other hand, installation of a TPV system could reduce radiative impact to the water cooled panels and convert a part of the radiative heat to electrical energy with sufficient efficiency. To demonstrate the effect of different EAF conditions on TPV performance, a simulation based model was modified, that is, remodeling the radiative heat transfer module and adding a TPV module. The study has shown that a capacity factor of a TPV system could reach upon 54% (annually) and improves the overall efficiency of the EAF up to 0.8%.

Acknowledgement

The paper received funding from Sharif Research Energy Institute (SERI), project *Simulation and control of an EAF*. The support of SERI is kindly acknowledged.

Appendix

Table A1. VF equations used in radiative heat transfer module.[22]

Case	Equation
Interior of the Outer Cylinder to itself with Inner Coaxial Cylinder	$VF = 1 - \frac{1}{R^*} + \frac{2}{\pi R^*}\tan^{-1}\left(\frac{2\left(R^{*2}-1\right)^{.5}}{l^*}\right) -$
Interior of the Outer Cylinder to Inner Coaxial Cylinder	$VF = \frac{1}{R^*} -$
Where	$R^* = \frac{R_{OuterCylinder}}{R_{InnerCoaxialCylinder}}$ $\quad l^* = \frac{l}{R_{Inner\ \ Coaxial\ \ Cylinder}}$
	$a = l^{*2} + R^{*2} - 1$ $\quad b = l^{*2} - R^{*2} + 1$
Outer Surface of the Cylinder to Angular Disk at the End of the Cylinder	$VF = \frac{\gamma_2}{8R^*l^*}^{***} +$
	$\frac{1}{2\pi}\left[\cos^{-1}\left(\frac{\gamma_1}{\gamma_2}\right) - \frac{1}{2l^*}\left(\frac{(\gamma_1+2)^2}{R^{*2}}-4\right)^{.5}\cos^{-1}\left(\frac{\gamma_1 R^*}{\gamma_2}\right) - \frac{\gamma_1}{2R^*l^*}\sin^{-1}(R^*)\right]$
Where	$R^* = \frac{R_{Inner\ \ Coaxial\ \ Cylinder}}{R_{Annular\ \ Disk}}$ $\quad l^* = \frac{l}{R_{Annular\ \ Disk}}$
	$\gamma_1 = l^{*2} + R^{*2} - 1$ $\quad \gamma_2 = l^{*2} - R^{*2} + 1$

*** γ_2 is mistyped γ_1 in ref.[22]

Keywords

Electric arc furnace, Heat recovery, Radiative heat transfer, Thermophotovoltaic system, Water-cooled panels

Final Version: January 9, 2018
Received: October 23, 2017
Published online:

[1] H. Rubel, M. Wortler, F. Schuler, R. Micha, *Sustainable Steelmaking-Meeting Today's Challenges, Forging Tomorrow's Solutions*, The Boston Consulting Group, Dussledorf, **2009**.
[2] *Fact Sheet: Energy use in the steel industry*, World steel association, Belgium **2014**.
[3] K. Gandt, T. Meier, T. Echterhof, H. Pfeifer, *Ironmaking Steelmaking* **2016**, *43*, 581.
[4] B. Lee, I. Sohn, *JOM* **2014**, *66*, 1581.
[5] M. Kirschen, V. Risonarta, H. Pfeifer, *Energy* **2009**, *34*, 1065.
[6] Ü. Çamdali, M. Tunç, *Appl. Therm. Eng.* **2003**, *23*, 2255.
[7] F. Bouzid, L. Dehimi, *Rev. Energies Renouvelables* **2012**, *15*, 383.
[8] J. F. Moynihan, P. F. Baldasaro, B. C. Campbell, C. A. Wang, H. K. Choi, G. W. Turner, S. J. Wojtczuk, P. Colter, P. Sharps, M. Timmons, R. E. Fahey, K. Zhang, *J. Electron. Mater.* **1998**, *27*, 1038.
[9] M. Mauk, in *Mid-infrared Semiconductor Optoelectronics* vol. *118* (Ed: A. Krier), Springer, London, **2006**, pp. 673–738.
[10] M. Mauk, V. Andreev, *Semicond. Sci. Technol* **2003**, *18*, S191.
[11] T. Bauer, *Thermophotovoltaics: Basic Principles and Critical Aspects of System Design*: Springer Science & Business Media, Berlin, Germany **2011**.
[12] T. Bauer, I. Forbes, N. Pearsall, *Int. J Ambient Energy* **2004**, *25*, 19.
[13] Z. Utlu, U. Parali, *Energy Convers. Manag.* **2013**, *74*, 308.
[14] T. Bauer, I. Forbes, R. Penlington, N. Pearsall, in *Fifth Conference on Thermophotovoltaic*, American Institute of Physics, Rome **2003**.
[15] L. M. Fraas, in *Photovoltaic Specialist Conference (PVSC)*, 2014 IEEE 40th, Denver, USA **2014**, pp. 0766–0770.
[16] A. Fathi, Y. Saboohi, I. Škrjanc, V. Logar, *Steel Res. Int.* **2017**, *88*, 1.
[17] G. Mattarolo, *Development and Modelling of a Thermophotovoltaic System*, *vol. 8*, Kassel University Press GmbH, Kassel, Germany **2007**.
[18] F. Opitz, P. Treffinger, J. Wöllenstein, *Metall. Mater. Trans. B*, **2017**, *48*, 3301.
[19] V. Logar, I. Škrjanc, *ISIJ Int.* **2012**, *52*, 1225.
[20] R. D. M. MacRosty, C. L. E. Swartz, *Ind. Eng. Chem. Res.* **2005**, *44*, 8067.
[21] F. Qian, B. Farouk, R. Mutharasan, *Metall. Mater. Trans. B* **1995**, *26*, 1057.
[22] M. Kaviany, *Essentials of Heat Transfer: Principles, Materials, and Applications*, Cambridge University Press, New York, USA **2011**.
[23] A. Fathi, Y. Saboohi, I. Škrjanc, V. Logar, *ISIJ Int.* **2015**, *55*, 1353.
[24] D. Chubb, *Fundamentals of Thermophotovoltaic Energy Conversion*, Elsevier, Amsterdam, Netherlands; Oxford, UK **2007**.
[25] C. M. Waits, *Thermophotovoltaic Energy Conversion for Personal Power Sources,* Army Research Lab Adelphi Md Sensors and Electron Devices Directorate, Adelphi, Maryland, USA **2012**.
[26] L. Fraas, L. Minkin, in *Thermophotovoltaic Generation of Electricity-(AIP Conference Proceedings Volume 890)* **2007**, pp. 17–23.
[27] J. Huwaldt, PLOT DIGITIZER 2.5. 0. Open source software. See http, plotdigitizer. sourceforge.net, **2010**.
[28] A. Kwon, *Electric generator capacity factors vary widely across the world*, **2015**. https://www.eia.gov/todayinenergy/detail.php?id=22832.
[29] C. Ferrari, F. Melino, M. Pinelli, P. R. Spina, M. Venturini, *Energy Procedia* **2014**, *45*, 160.
[30] L. Honorio, *Efficiency in Electricity Generation. Eurelectric: Union of the Electric Industry, VGB Powertech*, Brussels, Belgium **2003**.
[31] W. Cole, T. Mai, J. Logan, D. Steinberg, J. McCall, J. Richards, B. Sigrin, G. Porro, 2016 Standard Scenarios Report: A US Electricity Sector Outlook, NREL (National Renewable Energy Laboratory (NREL), Golden, CO **2016**.